

Enhanced diffusion of tracer particles in nonreciprocal mixtures

Anthony Benois,¹ Marie Jardat,¹ Vincent Dahirel,¹ Vincent Démery,^{2,3}
Jaime Agudo-Canalejo,⁴ Ramin Golestanian,^{4,5} and Pierre Illien¹

¹*Sorbonne Université, CNRS, Physico-Chimie des Électrolytes et
Nanosystèmes Interfaciaux (PHENIX), 4 Place Jussieu, 75005 Paris, France*

²*Gulliver, UMR CNRS 7083, ESPCI Paris PSL, 75005 Paris, France*

³*Université Lyon, ENS de Lyon, Université Claude Bernard,*

CNRS, Laboratoire de Physique, F-69342 Lyon, France

⁴*Department of Living Matter Physics, Max Planck Institute for Dynamics and Self-Organization, D-37077 Göttingen, Germany*

⁵*Rudolf Peierls Centre for Theoretical Physics, University of Oxford, OX1 3PU, Oxford, UK*

(Dated: November 20, 2023)

We study the diffusivity of a tagged particle in a binary mixture of Brownian particles with non-reciprocal interactions. Numerical simulations reveal that, for a broad class of interaction potentials, non-reciprocity can significantly increase the long-time diffusion coefficient of tracer particles, and that this diffusion enhancement is associated with a breakdown of the Einstein relation. These observations are quantified and confirmed via two different and complementary analytical approaches: (i) a linearized stochastic density field theory, which is particularly accurate in the limit of soft interactions; (ii) a reduced two-body description, which is exact at leading order in the density of particles. The latter reveals that diffusion enhancement can be attributed to the formation of transiently propelled dimers of particles, whose cohesion and speed are controlled by the non-reciprocal interactions.

I. INTRODUCTION

Intracellular functions are governed by the transport of ions, proteins, vesicles, or organelles, which are subject to strong thermal fluctuations, and which interact with each other through crowding, electrostatics and hydrodynamics. In theoretical approaches, such systems are typically represented by a suspension of interacting particles, embedded in a solvent that causes their stochastic motion. These particles generally evolve very far from equilibrium, and are ‘active’ in the sense that they locally convert the chemical energy available in their environment into mechanical work. Even though a wealth of knowledge has been gathered on suspensions of single-species ‘polar’ or self-propelled active particles [1–4], the reality is much more complex: suspensions of biological interest are generally strongly heterogeneous, and made of particles without any established polarity on the considered timescales.

Very recently, ‘scalar’ models for active matter, where agents are apolar but whose nonequilibrium dynamics results in spontaneous symmetry breaking, have been developed. For instance, one can consider catalytic molecules, such as proteins or enzymes, that are involved in the production or consumption of smaller solute molecules. Each of them can be seen as a local source or sink responding to the chemical gradients created by the other particles. When coarse-graining the degrees of freedom associated with solute molecules, the effective interactions between particles appear to break action-reaction symmetry [5–8], and should be modeled as non-reciprocal. This line of research has recently gained a lot of importance, and now goes well beyond the interest for active colloids, with applications ranging from the design of new field theories [9–11] and advanced sampling

techniques [12], to the interpretation of active matter experiments [13–16], and more generally phase transitions in nonequilibrium systems [17]. Interestingly, mixtures of particles with non-reciprocal interactions can be mapped onto multi-temperature suspensions – another class of scalar active matter that have received a lot of interest in the soft matter and biophysics communities [18–23]. This mapping was formally established for Newtonian dynamics [24], and can be extended to stochastic overdamped dynamics (see Appendix A).

The collective and structural properties of non-reciprocal mixtures have been studied rather extensively, revealing in particular their tendency to phase separate [7, 25, 26]. However, the properties of their fluctuations, as characterized by the dynamics of tracer particles (i.e. individually-tracked, tagged particles) have been left aside so far, in spite of their importance. Indeed, the properties of tagged particles generally contain key information about the microstructure of the suspension and its small-scale dynamics [27]. They are also of importance to quantify experiments that rely on single-particle tracking and allow accurate characterization of many intracellular processes [28].

In this article, we study the diffusivity of a tagged particle in a binary mixture of particles with non-reciprocal interactions obeying overdamped Langevin dynamics. Brownian dynamics simulations, together with two different analytical treatments of the stochastic dynamics, reveal that non-reciprocity can significantly increase the effective long-time diffusion coefficient of tracer particles. We measure the non-reciprocal contribution to its diffusivity:

$$D_{\text{eff}} = D_{\text{recip}} + \Delta D_{\text{non-recip}}, \quad (1)$$

and, we show that, strikingly, this diffusion enhance-

ment is associated with a breakdown of the Einstein relation, which does not hold in this nonequilibrium case. More precisely, the effective long-time mobility can be written as $\mu_{\text{eff}} = D_{\text{recip}}/k_B T + \Delta\mu_{\text{non-recip}}$, with the non-reciprocal correction being generally different from $\Delta D_{\text{non-recip}}/k_B T$. We finally show that diffusion enhancement can be attributed to the formation of transiently propelled dimers of particles, whose cohesion and speed are controlled by the non-reciprocal interactions.

II. MODEL

We consider a three-dimensional binary suspension of $N + 1$ interacting particles, made of N_A (resp. N_B) particles of species A (resp. B), and one tracer particle (labeled 0), that can either be of type A or of type B . We denote by $\rho_\alpha = N_\alpha/V$ ($\alpha = A$ or B) the number density of each species (excluding the tracer), where V is the volume of the system. The overall density of bath particles is $\rho = N/V$, and $X_\alpha = \rho_\alpha/\rho$ is the fraction of α particles [29]. We assume that each particle obeys an overdamped Langevin dynamics, in such a way that the evolution of the system is given by the set of coupled equations:

$$\frac{d\mathbf{r}_n}{dt} = \mu_{S(n)} \sum_{m \neq n} \mathbf{F}_{S(m) \rightarrow S(n)}(\mathbf{r}_n - \mathbf{r}_m) + \sqrt{2D_{S(n)}} \boldsymbol{\zeta}_n(t), \quad (2)$$

where $S(n) \in \{A, B\}$ denotes the species of particle n , and $\mathbf{F}_{\beta \rightarrow \alpha}(\mathbf{r})$ denotes the force exerted by a particle of species β on a particle of species α when the latter is located at \mathbf{r} relative to the former. The bare diffusion coefficient of a particle of species α is related to the mobility μ_α through the Einstein relation $D_\alpha = k_B T \mu_\alpha$, where T is the temperature of the thermal bath in which the particles are embedded. For simplicity, we will assume that all the particles have the same mobility μ_0 . The noise terms $\boldsymbol{\zeta}_n(t)$ have zero average and are delta-correlated: $\langle \zeta_{n,i}(t) \zeta_{m,j}(t') \rangle = \delta_{nm} \delta_{ij} \delta(t - t')$.

Importantly, we assume that the interactions between particles of different species can be non-reciprocal, namely that $\mathbf{F}_{A \rightarrow B}(\mathbf{r}) \neq -\mathbf{F}_{B \rightarrow A}(-\mathbf{r})$. In order to probe the existence of enhanced diffusion in such a suspension, we compute the long-time diffusion coefficient of the tracer particle, defined as $D_{\text{eff}} = \lim_{t \rightarrow \infty} \langle |\mathbf{r}_0(t) - \mathbf{r}_0(0)|^2 \rangle / 6t$.

For simplicity, we write the forces as deriving from potentials (or ‘pseudo-potentials’): $\mathbf{F}_{\alpha \rightarrow \beta}(\mathbf{r}_\beta - \mathbf{r}_\alpha) = -\nabla_{\mathbf{r}_\beta} \phi_{\alpha \rightarrow \beta}(|\mathbf{r}_\alpha - \mathbf{r}_\beta|)$. Note that we thus focus on divergence-free force fields. With this definition, the pseudo-potentials correspond to regular pair potentials when $\alpha = \beta$, but not otherwise. The interactions between species can be defined through a matrix with elements $\Phi_{\alpha\beta} = \phi_{\alpha \rightarrow \beta}$ which is split between a symmetric

(reciprocal) and antisymmetric (nonreciprocal) part:

$$\Phi = \begin{pmatrix} \phi_{\text{rep}} & \phi_{\text{rep}} \\ \phi_{\text{rep}} + \phi_{\text{att}} & \phi_{\text{rep}} \end{pmatrix} \quad (3)$$

$$= \begin{pmatrix} \phi_{A \rightarrow A} & \phi_{AB}^R \\ \phi_{AB}^R & \phi_{B \rightarrow B} \end{pmatrix} + \begin{pmatrix} 0 & -\phi_{AB}^{\text{NR}} \\ \phi_{AB}^{\text{NR}} & 0 \end{pmatrix}. \quad (4)$$

For concreteness, we assume that all the (α, β) pairs interact via a purely repulsive potential $\phi_{\text{rep}}(r)$, and that non-reciprocity is incorporated by assuming that the pseudo-potential $\phi_{A \rightarrow B}$ contains an additional attractive part $\phi_{\text{att}}(r)$ (in the notations of Eq. (4), this means that $\phi_{AB}^R = \phi_{\text{rep}} + \phi_{\text{att}}/2$ and $\phi_{AB}^{\text{NR}} = \phi_{\text{att}}/2$).

III. NUMERICAL EVIDENCE FOR ENHANCED DIFFUSION

A. Main results

We first present results from Brownian dynamics simulations, which consist in integrating the set of coupled overdamped Langevin equations [Eq. (2)], using a forward Euler-Maruyama scheme (see Appendix B). We consider different types of binary mixtures and the corresponding pair potentials, that represent a broad range of physical situations (for each system, the expressions of ϕ_{rep} and ϕ_{att} are given in Table I): (i) suspensions of hard particles with short-range repulsion given by the Weeks-Chandler-Andersen potential and long-range Lennard-Jones attraction [25, 26]; (ii) particles with softcore interactions, modeled by a ‘Gaussian’ potential, which are relevant to describe the interactions between polymer coils [30–32]; and (iii) Yukawa interactions, that represent screened Coulomb interactions or may arise from ‘chemical interactions’ between diffusiophoretic colloids [5–7, 16] (the ranges λ and λ' of the Yukawa-like ϕ_{rep} and ϕ_{att} are chosen such that $\phi_{A \rightarrow B}$ has an attractive part). For all these systems, the energy parameters ε and δ represent respectively the strength of the repulsive and attractive parts of the potentials. When non-reciprocity is very strong, the suspension may be unstable and phase separate – this effect was for instance evidenced in suspensions of colloids with chemically-mediated [7] or LJ-WCA [25, 26] interactions. However, we emphasize that all our simulations are performed in the homogeneous regime, where the non-reciprocal mixture does not display any phase separation.

In each of these systems, we measure numerically the diffusion coefficient of tagged B particles, as summarized in Fig. 1. For all three sets of simulations, diffusion is enhanced as non-reciprocity increases (a similar effect is observed for tagged A particles, see Appendix C). In the particular case of the softcore potentials, the relative enhancement can reach values as high as 20% [33]. The radial distribution functions reveal a strong pairing between A and B particles (Appendix C), which is interpreted as a consequence of the ‘predator-prey’ dynamics

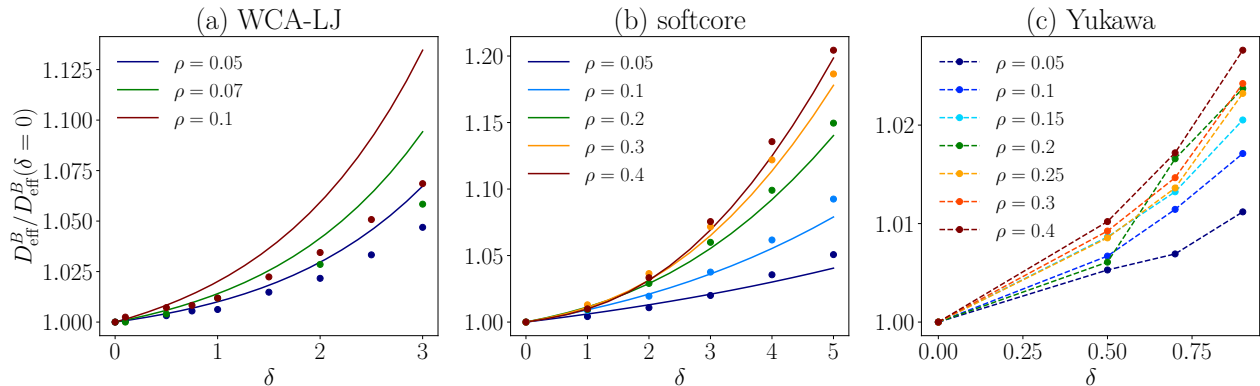


FIG. 1. Long-time diffusion coefficients of B particles (rescaled by their value in the reciprocal case, $\delta = 0$) as a function of the parameter δ , which quantifies the intensity of non-reciprocity. Throughout the paper, energies are measured in units of $k_B T$ and distances in units of σ , the diameter of the particles. In all simulations, and unless otherwise specified, $\rho_A = \rho_B = \rho/2$. (a) solid lines are analytical predictions in the low-density limit (Appendix F); (b) solid lines are analytical predictions in the limit of soft interactions [Eq. (6)]; (c) dashed lines are guides to the eye. See Table I for the expressions of the pair potentials (parameters: $\varepsilon = 1$, $\sigma = 1$, $\lambda = 1$, $\lambda' = 1.7$).

	$\phi_{\text{rep}}(r)$	$\phi_{\text{att}}(r)$
LJ-WCA	$4\varepsilon \left[\left(\frac{\sigma}{r}\right)^{12} - \left(\frac{\sigma}{r}\right)^6 \right] \theta(2^{1/6}\sigma - r)$	$4\delta \left[\left(\frac{\sigma}{r}\right)^{12} - \left(\frac{\sigma}{r}\right)^6 \right]$
softcore	$\varepsilon e^{-(r/\sigma)^2}$	$-\delta e^{-(r/\sigma)^2}$
Yukawa	$\varepsilon \frac{\sigma}{r} e^{-r/\lambda}$	$-\delta \frac{\sigma}{r} e^{-r/\lambda'}$

TABLE I. Expressions of the repulsive and attractive part of the interaction potentials considered in the simulations.

that emerges from non-reciprocal interactions: B particles chase A particles while A tend to run away from B , resulting in enhanced dynamics at the scale of tagged particles – this effect will be described in Section VI.

B. Additional comments

We emphasize that choosing another decomposition of the matrix Φ [Eq. (4)] is not expected to affect the main results. Non-reciprocity is controlled by the intensity of the pseudo-potential ϕ_{att} (through the parameter δ), which is independent of the decomposition into a reciprocal and a non-reciprocal part. There are possibly other choices of the decomposition that would surely modify the ‘enhancement’, if we change the reference with respect to which diffusion coefficient is measured, but we argue that, in the present situation, the best choice to rationalize our simulation results is to take $D_{\text{eff}}(\delta = 0)$ as a reference.

Finally, it is interesting to think about the relevant observables that should be used to discriminate between reciprocal or non-reciprocal interactions in experimental measurements. As the diffusion coefficient of a tagged particle can be larger or smaller depending on the sign of

δ , we believe that the diffusion coefficient would probably not be a sufficient observable to identify the reciprocal case. The measurement of diffusion coefficients could be completed by observables that characterize the structure and spatial organization of the system, in which the signature of the pairing mechanism can be observed (see for instance the radial distribution functions shown on Fig. 4).

IV. BREAKDOWN OF THE EINSTEIN RELATION

In order to probe the validity of the Einstein relation in such mixtures, we measured the mobility of tagged particles, aiming at comparing it to the effective diffusion coefficient defined earlier. To this end, in the numerical simulations, we add a constant external force $\mathbf{f} = f\mathbf{e}_x$ to the tagged particle, and measure its mobility defined as $\mu_{\text{eff}} = \lim_{f \rightarrow 0} \langle v_x \rangle / f$, where $\langle v_x \rangle$ is the average velocity attained by the tagged particle along direction x , in the stationary limit. For an equilibrium system, the effective mobility of the tracer is expected to be related to its effective diffusion coefficient through the Einstein relation $D_{\text{eff}} = k_B T \mu_{\text{eff}}$. We compare in Fig. 2 the effective diffusion coefficients and mobilities as measured from simulations: the increasing mismatch between their values as δ increases is a clear indication of the breakdown of the Einstein relation in this nonequilibrium situation.

V. ANALYTICAL DESCRIPTION IN THE LIMIT OF SOFT INTERACTIONS

In order to quantify these phenomena and to offer analytical insight, we coarse-grain the dynamics and define the density of bath particles of species α as $\hat{\rho}_\alpha(\mathbf{r}, t) =$

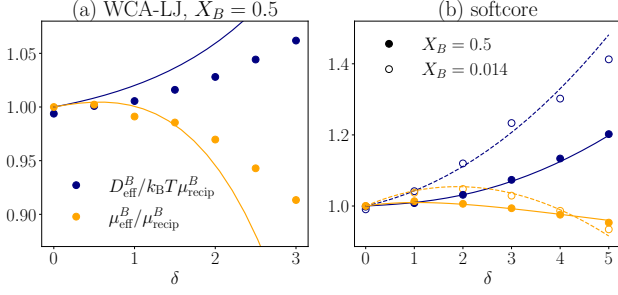


FIG. 2. Long-time diffusion coefficients and mobilities of tagged B particles in non-reciprocal mixtures as a function of the parameter δ . Densities are (a) $\rho = 0.10$; (b) $\rho = 0.40$ (see caption of Fig. 1 for the other parameters). In both panels, symbols are results from Brownian dynamics simulations. (a) Solid lines are analytical predictions in the low-density limit (Appendix F). (b) Solid and dashed lines are analytical predictions in the limit of soft interactions [see Eq. (6) for D_{eff}^B and Eq. (D50) for μ_{eff}^B].

$\sum_{n \neq 0, S(n)=\alpha} \delta(\mathbf{r}_n(t) - \mathbf{r})$, where the sum runs over all the particles of species α except the tracer (if of species α), so that the tracer is ‘taken out’ of the definition of the densities [34]. Using Itô calculus [35], and relying on the usual derivation proposed by Dean for a single-component fluid [36] and later extended to binary mixtures [37], we obtain the coupled equations for the fields $\hat{\rho}_\alpha$:

$$\begin{aligned} \partial_t \hat{\rho}_\alpha &= \sqrt{2D_0} \nabla \cdot [\boldsymbol{\eta}_\alpha \sqrt{\hat{\rho}_\alpha}] + D_0 \nabla^2 \hat{\rho}_\alpha \\ &- \mu_0 \nabla \cdot \left[\hat{\rho}_\alpha \sum_{\beta \in \{A, B\}} \mathbf{F}_{\beta \rightarrow \alpha} * \hat{\rho}_\beta + \hat{\rho}_\alpha \mathbf{F}_{S(0) \rightarrow \alpha} * \delta_{\mathbf{r}_0} \right] \end{aligned} \quad (5)$$

with the space-dependent noise $\eta_{\alpha,i}(\mathbf{r}, t)$ of average zero, and with correlations $\langle \eta_{\alpha,i}(\mathbf{r}, t) \eta_{\beta,j}(\mathbf{r}', t') \rangle = \delta_{\alpha\beta} \delta_{ij} \delta(\mathbf{r} - \mathbf{r}') \delta(t - t')$. In Eq. (5), the symbol $*$ represents spatial convolution: $(f * g)(\mathbf{r}) = \int d\mathbf{r}' f(\mathbf{r}') g(\mathbf{r} - \mathbf{r}')$, and we use the shorthand notation $\delta_{\mathbf{r}_0}(\mathbf{r}) = \delta(\mathbf{r} - \mathbf{r}_0)$. The evolution of the tracer position is given by the overdamped Langevin equation, Eq. (2), written for $n = 0$.

Although explicit, this joint description of the tracer-bath dynamics is quite complicated, as it involves nonlinear couplings and multiplicative noise. The dynamics of the fields can be solved perturbatively by linearizing around the homogeneous state of density ρ_α , and assuming $|\hat{\rho}_\alpha - \rho_\alpha| \ll \rho_\alpha$ [34, 37]. To treat the nonlinear coupling between the fields and the position of the tracer $\mathbf{r}_0(t)$, we rely on a path-integral formulation [38] that we recently extended to the case of a binary mixture [39]. We finally reach an expression for the long-time diffusion

coefficient of the tracer particle as a Fourier integral:

$$\begin{aligned} \frac{D_{\text{eff}}}{D_0} &= 1 - \sum_{\substack{\alpha, \beta, \gamma \\ \in \{A, B\}}} \sqrt{X_\alpha X_\gamma} \int_0^\infty \frac{dq}{6\pi^2} \rho q^2 \tilde{\phi}_{\alpha \rightarrow S(0)}(q) \\ &\times \left[C_{S(0) \rightarrow \gamma}^{\alpha\beta\gamma} \tilde{\phi}_{S(0) \rightarrow \gamma}(q) + C_{\gamma \rightarrow S(0)}^{\alpha\beta\gamma} \tilde{\phi}_{\gamma \rightarrow S(0)}(q) \right] \end{aligned} \quad (6)$$

where the tildes represent Fourier transforms, and where the functions $C_{S(0) \rightarrow \gamma}^{\alpha\beta\gamma}(q)$ and $C_{\gamma \rightarrow S(0)}^{\alpha\beta\gamma}(q)$ are given in Appendix D in terms of the densities of each species, their interaction potentials, and their mobilities (note that, in that Appendix, we actually consider the more general situation where the tracer can be a different species than A or B). Additionally, the long-time effective mobility of the tracer particle can be computed with similar tools: technically, this is done by applying a small external force \mathbf{f} to the tracer and computing the correction to the average tracer velocity (Appendix D3) [34].

Eq. (6) is one of the main analytical results of this article, and several comments follow: (i) Up to a numerical integration, the effective long-time diffusion coefficient is obtained as an explicit expression in terms of all the parameters of the problem; (ii) In our formalism, one can actually find a more general expression of the effective long-time diffusion coefficient, for cases in which A and B particles have different mobilities and are connected to different thermostats (Appendix D); and (iii) This result should be understood as a perturbative expansion in the limit of weak interactions between the particles. Therefore, when compared to our numerical results for the different interaction potentials considered in Table I, it is only valid for the softcore interactions: the agreement between our analytical theory and numerical simulations is very good [Fig. 1(b)]. Strikingly, it shows that this linearization procedure remains true even very far from equilibrium.

In order to discuss some consequences of Eq. (6), we consider a simpler situation, where the tagged particle is coupled in a non-reciprocal way to a single bath (we will assume that the probe is of species B and the bath particles of species A). We take $\phi_{A \rightarrow A}(r) = \phi_{B \rightarrow A}(r) = v(r)$ and $\phi_{A \rightarrow B}(r) = (1 - \delta)v(r)$, in such a way that δ measures non-reciprocity, just like in our numerical simulations. In this case, the effective long-time diffusion coefficient of the tagged particle has the simple expression:

$$D_{\text{eff}} = D_{\text{recip}} + D_0 \int \frac{d\mathbf{q}}{(2\pi)^3} \frac{\rho \delta (2 + \delta \rho \tilde{v}) \tilde{v}^2}{3(1 + \rho \tilde{v})(2 + \rho \tilde{v})^2}, \quad (7)$$

where $\frac{D_{\text{recip}}}{D_0} = 1 - \frac{\rho}{3} \int \frac{d\mathbf{q}}{(2\pi)^3} \frac{\tilde{v}^2}{(1 + \rho \tilde{v})(2 + \rho \tilde{v})}$. The effective mobility of the tracer can be computed by assuming that it is driven by a harmonic trap with vanishing stiffness, and by adapting earlier calculations [40]. We find that the effective mobility is given by

$$\mu_{\text{eff}} = \frac{D_{\text{recip}}}{k_B T} + \mu_0 \int \frac{d\mathbf{q}}{(2\pi)^3} \frac{\rho \delta (3 - \delta + \delta \rho \tilde{v}) \tilde{v}^2}{3(1 + \rho \tilde{v})(2 + \rho \tilde{v})^2}, \quad (8)$$

which we compare to numerical data in Fig. 2(b). Therefore, this confirms the breakdown of the Einstein relation, which is only retrieved in the reciprocal case $\delta = 0$ and the trivial case $\delta = 1$, where the bath has no effect on the tracer.

VI. LOW-DENSITY LIMIT

We finally consider the low-density limit of the problem, where it actually reduces to a two-particle situation: one of them is the tagged particle, the other one is a bath particle. To ease the notation, we will assume that the tracer, at position \mathbf{r}_0 , is of species α , and the considered bath particle, at position \mathbf{r}_b , is of species β . The pair correlation of the tracer with the bath particle is obtained by solving the Smoluchovski equation for the two-body probability density $P_{\alpha\beta}(\mathbf{r}_0, \mathbf{r}_b, t)$. Using the variables $\mathbf{r} = \mathbf{r}_b - \mathbf{r}_0$ and $\mathbf{R} = (\mathbf{r}_0 + \mathbf{r}_b)/2$, it reads

$$\begin{aligned} \partial_t P_{\alpha\beta} &= 2D_0 \nabla_{\mathbf{r}}^2 P_{\alpha\beta} + \mu_0 \nabla_{\mathbf{r}} \cdot [P_{\alpha\beta} \nabla_{\mathbf{r}} (\phi_{\alpha\rightarrow\beta} + \phi_{\beta\rightarrow\alpha})] \\ &+ \frac{D_0}{2} \nabla_{\mathbf{R}}^2 P_{\alpha\beta} + \frac{\mu_0}{2} \nabla_{\mathbf{R}} P_{\alpha\beta} \cdot \nabla_{\mathbf{r}} (\phi_{\beta\rightarrow\alpha} - \phi_{\alpha\rightarrow\beta}). \end{aligned} \quad (9)$$

Integrating over the position of the center of mass \mathbf{R} , and defining $u_{\alpha\beta}(r) = [\phi_{\alpha\rightarrow\beta}(r) + \phi_{\beta\rightarrow\alpha}(r)]/2k_B T$, we find the stationary solution of Eq. (9): $g_{\alpha\beta}^0(r) = \exp[-u_{\alpha\beta}(r)]$. Interestingly, this is analogous to the simple equilibrium pair distribution in the low-density limit, but with the interaction potential taken as the average between the two non-reciprocal pseudo-potentials. The long-time diffusion coefficient of the tracer, as well as its effective mobility, can be computed using standard methods [41, 42], and the comparison between these two observables shows that the Einstein relation does not hold in this limit either (see Appendix F). Although the potentials used in this study do not allow the derivation of explicit expressions for the long-time diffusion coefficient and mobility in this limit, we can evaluate through the numerical resolution of ordinary differential equations. For LJ/WCA potentials, the results are shown on Fig. 1(a), Fig. 2(a) and Fig. 3(a).

This low-density approach also reveals that, if the effective potential $u_{\alpha\beta}(r)$ has a deep enough minimum, an $\alpha\beta$ pair may form a ‘transient dimer’ that remains bound for some time. Indeed, the dynamics of their center of mass \mathbf{R} can be read from the effective equation of motion $\dot{\mathbf{R}}(t) = \frac{\mu_0}{2} \nabla (\phi_{\alpha\rightarrow\beta} - \phi_{\beta\rightarrow\alpha}) + \sqrt{D_0} \boldsymbol{\xi}(t)$, where $\boldsymbol{\xi}(t)$ is a Gaussian white noise with unit variance. If the interaction is non-reciprocal, the first term on the r.h.s. is non-zero and represents a self-propulsion term, which depends solely on the inner variable $\mathbf{r}(t)$. The characteristics of self-propulsion depend on the shape of the potentials: (i) If the minimum of $u_{\alpha\beta}(r)$ is at $r = 0$ and the potentials behave as $\phi_{\alpha\beta}(r) \sim k_{\alpha\beta} r^2/2$ around $r = 0$, then the dynamics of $\mathbf{r}(t)$ is linear, $\mathbf{r}(t)$ is an Ornstein-Uhlenbeck process, and the coordinate $\mathbf{R}(t)$ therefore behaves as an Active Ornstein-Uhlenbeck particle [43]; (ii)

On the contrary, if the minimum of $u_{\alpha\beta}(r)$ is at $r^* > 0$, then the modulus of interparticle vector remains confined close to r^* , and one can define a self-propulsion velocity $V_0 \simeq \frac{D_0}{2} [\phi'_{\alpha\beta}(r^*) - \phi'_{\beta\alpha}(r^*)]$: the coordinate $\mathbf{R}(t)$ behaves as an Active Brownian Particle [44], with a rotational diffusion coefficient $D_r \simeq 2D_0/r^{*2}$.

In our numerical simulations, when the overall density ρ is small enough, we observe that $D_{\text{eff}}^A \simeq D_{\text{eff}}^B$, even for strong non-reciprocity (Appendix C). In contrast, at higher densities, these two values differ more clearly. This supports the idea that, at low density, diffusion enhancement can be related to the pairing between A and B particles. This effect is reminiscent of the self-propelled dimers observed in very dilute suspensions of chemotactic colloids [5, 13, 15, 16]. This relationship between the nonreciprocal mixture and suspensions of active particles (Brownian or Ornstein-Uhlenbeck) could be used to define an ‘active temperature’ and a generalized Einstein relation [45].

VII. DISCUSSION

In this article, we showed that non-reciprocal interactions between Brownian particles could significantly enhance their diffusivity. Non-reciprocity, which plays a predominant role in the interaction between chemically active particles, is thus expected to have a significant impact on the efficiency of molecular transport, and on the kinetics of diffusion-limited reactions. These observations, together with the mapping between non-reciprocal and two-temperature mixtures, open the way to the interpretation of the rich phenomenology of non-reciprocal and multi-temperature mixtures, and to the local structures that emerge from the local energy transfers at the microscopic scale [46]. In the biological context, we believe that these concepts could find their applications in elucidating the role played by ATP-fueled activity in the fluidization of the intracellular medium, and of its rheological properties [47].

ACKNOWLEDGMENTS

The authors acknowledge Roxanne Berthin for her assistance with the computational resources of PHENIX laboratory, and Rodrigo Soto for discussions.

DATA AVAILABILITY

The input files and raw data used for the figures are available on Zenodo (<https://doi.org/10.5281/zenodo.10126206>).

Appendix A: Mapping from multi-temperature suspensions to non-reciprocal mixtures

The mapping from multi-temperature suspensions to non-reciprocal mixtures was demonstrated for a binary, underdamped suspension in Ref. [24]. We extend here these arguments for an arbitrary number of species, in the overdamped limit. We write the generic Smoluchowski equation for a suspension of N particles connected to N different thermostats:

$$\partial_t \mathcal{P}(\mathbf{r}^N; t) = \sum_{n=1}^N \left\{ k_B T_n \mu_n \nabla_{\mathbf{r}_n}^2 \mathcal{P}(\mathbf{r}^N; t) - \mu_n \nabla_{\mathbf{r}_n} \left[\mathcal{P}(\mathbf{r}^N; t) \sum_{m \neq n} \mathbf{F}(\mathbf{r}_n - \mathbf{r}_m) \right] \right\}, \quad (\text{A1})$$

where μ_n is the mobility of particle n , T_n its temperature, \mathbf{F} is a reciprocal force field (reciprocal in the sense that it depends only on the distance between the particles, and not on their species), and $\mathcal{P}(\mathbf{r}^N; t)$ is the N -body probability distribution (we use the shorthand notation: $\mathbf{r}^N = (\mathbf{r}_1, \dots, \mathbf{r}_N)$). It is straightforward to show that this equation also describes the dynamics of a suspension of N particles connected to a single thermostat T , but with mobilities $\mu'_n = (T_n/T)\mu_n$, and interacting via ‘non-reciprocal forces’ $\mathbf{F}_{m \rightarrow n}(\mathbf{r}_n - \mathbf{r}_m) = (T/T_n)\mathbf{F}(\mathbf{r}_n - \mathbf{r}_m)$ (here $\mathbf{F}_{m \rightarrow n}$ denotes the force exerted by particle m on particle n). Therefore, a mixture of overdamped particles with multiple temperatures can be mapped onto a mixture with non-reciprocal forces, but we underline that the converse is not always true. This gives additional justification for the study of non-reciprocal mixtures, that appears to be more general, and that they can give insight into the physics of multi-temperature systems.

Appendix B: Numerical methods

To perform Brownian dynamics simulations we have used the LAMMPS computational package [48–50]. We used the command ‘fix brownian’ that allows one to integrate overdamped Langevin equations for the positions of particles thanks to a forward Euler-Maruyama scheme. To allow the forces between A and B particles to be non-reciprocal, we have used Pylammeps, the wrapper python class for LAMMPS. More precisely, we have added in the simulation box a number of ‘ghost’ particles (named C in what follows) equal to that of A particles. The interaction potential between A and B is the interaction potential $\phi_{\text{rep}}(r)$, and C and B particles undergo the attractive interaction potential $\phi_{\text{att}}(r)$ (see Table I). At each time step of the simulation, ghost particles C are put at the exact same positions as particles A , so that they exert an additional attractive force on particles B as if they were A particles. This additional force does not influence particles A : as a result, the total force between

A and B particles are non-reciprocal. To compute interaction forces, cutoff distances equal to 2.5σ , 2.5σ , and 5σ are used for the Lennard-Jones, softcore and Yukawa interaction potentials, respectively. The input mobility of particles is the same for A and B particles.

In every case, a total number of $N_A = 2000$, $N_B = 2000$, $N_C = 2000$ particles are placed in a cubic simulation box with periodic boundary conditions. The length of the box L_{box} is varied to change the total density $\rho = (N_A + N_B)/L_{\text{box}}^3$ of the system. The time step varies between $\Delta t = 0.0002t^*$ and $\Delta t = 0.002t^*$, depending on the interaction potential and of the density of the system, with $t^* = \sigma^2/(k_B T \mu_0) = \sigma^2/D_0$ the time needed for a particle to diffuse over a length equal to its size. In each case, we begin by one long trajectory of 10^7 time steps to equilibrate the system at $\delta = 0$ (reciprocal case). For each value of δ , starting from a configuration representative of the equilibrium situation ($\delta = 0$), one long trajectory of about 10^7 time steps is run to reach a stationary state, characterized by constant radial distribution functions. Then, mean squared displacements of tracers are averaged over three to nine independent trajectories of about 10^7 time steps (depending on the time step and density), and over particles and time. The mean-squared displacements were found to be linear at all times for every system investigated here. The uncertainty of the computed self-diffusion coefficients was evaluated from the standard deviation of values obtained from different trajectories. The uncertainty on D_{eff}/D_0 was in each case smaller than 0.005. Note that the size of the symbols used in the figures is larger than these error bars.

Finally, to compute the mobility, we have added a force on 50 tracer B particles chosen at random. The amplitude of the force is chosen to ensure that we stay in the linear regime, i.e. the displacement with time is proportional to the force. Starting from equilibrated configurations obtained at each δ , we have run simulations of about 2×10^6 time steps with the added force. The mobility is computed from $\langle [\mathbf{r}(t) - \mathbf{r}(t=0)]/t \rangle$, averaging over the last 20% steps of three independent trajectories, and over the 50 tracer particles.

Appendix C: Additional results from Brownian dynamics simulations

In this Section, we present additional numerical results.

- We show in Fig. 3 the effective diffusion coefficient of A particles. This is the counterpart of Fig. 1, which showed the effective diffusion coefficient of B particles.
- We show in Fig. 4 the radial distribution functions for the different pairs of species in the binary mixtures (AA, BB, AB), and for the different interaction potentials used in the Brownian dynamics sim-

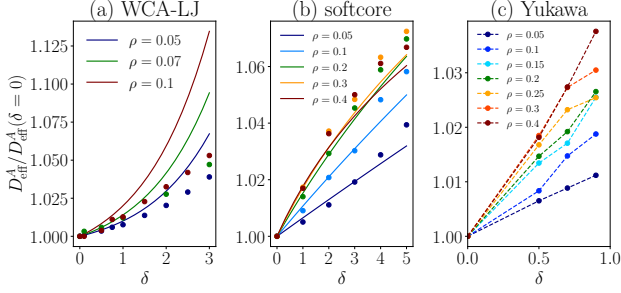


FIG. 3. Long-time diffusion coefficients of tagged A particles in non-reciprocal mixtures (rescaled by their value in the reciprocal case, $\delta = 0$) as a function of the parameter δ , which quantifies the intensity of non-reciprocity. Throughout the paper, energies are measured in units of $k_B T$ and distances in units of σ , the diameter of the particles. In all simulations, $\rho_A = \rho_B = \rho/2$. (a) solid lines are analytical predictions in the low-density limit (Appendix F 3); (b) solid lines are analytical predictions in the limit of soft interactions [Eq. (6)]; (c) dashed lines are guides to the eye. See Table I for the expressions of the pair potentials (parameters: $\varepsilon = 1$, $\sigma = 1$, $\lambda = 1$, $\lambda' = 1.7$).

ulations (WCA-LJ, softcore, Yukawa). The strong pairing between A and B particles is visible on the functions $g_{AB}(r)$, which are much larger than 1 when non-reciprocity is strong.

- We show in Fig. 5 the relative difference between the diffusion coefficients of A and B particles. More precisely, we define the diffusion coefficients rescaled by their reciprocal value: $\bar{D}_{\text{eff}}^\alpha = D_{\text{eff}}^\alpha / D_{\text{recip}}^\alpha$, and we define the relative difference between \bar{D}_{eff}^A and \bar{D}_{eff}^B as: $(\bar{D}_{\text{eff}}^B - \bar{D}_{\text{eff}}^A) / \frac{1}{2}(\bar{D}_{\text{eff}}^A + \bar{D}_{\text{eff}}^B)$. This quantity is plotted for the three sets of numerical simulations (LJ-WCA, softcore, Yukawa).

Appendix D: Limit of soft interactions

In the main text, for simplicity, we considered the situation where all the particles have the same mobilities, the same diffusion coefficients, and are connected to the same thermostat. We also assumed that the tracer was either a particle of species A , or a particle of species B . In this supplementary calculation, we consider the more general situation where the tracer, denoted by the index 0, can be a different species than A or B . There are *a priori* three different thermostats (T_0 , T_A and T_B), three different mobilities (μ_0 , μ_A and μ_B). The bare diffusion coefficients are related to temperatures and mobilities through the fluctuation-dissipation relation, which is assumed to hold in the limit of infinite dilution: $D_\alpha = k_B T_\alpha \mu_\alpha$. To ease the notation, we will denote by “0” the species of the

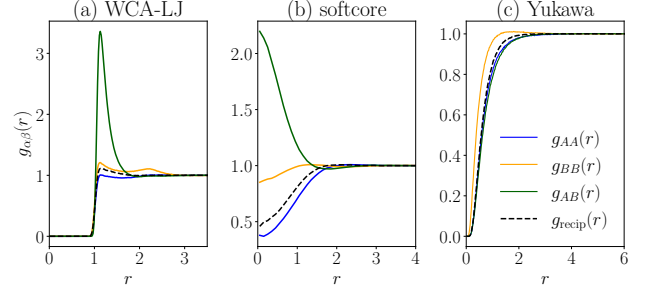


FIG. 4. Radial distribution functions for the different pairs of species in the binary mixtures (AA , BB , AB), and for the different interaction potentials used in the Brownian dynamics simulations (WCA-LJ: $\rho = 0.1$, $\delta = 3$, softcore: $\rho = 0.3$, $\delta = 5$, Yukawa: $\rho = 0.3$, $\delta = 0.9$). The curves for $g_{\text{recip}}(r)$ correspond to the AA radial distribution functions in the reciprocal case (the BB and AB radial distribution functions are identical within statistical noise, as expected in this situation).

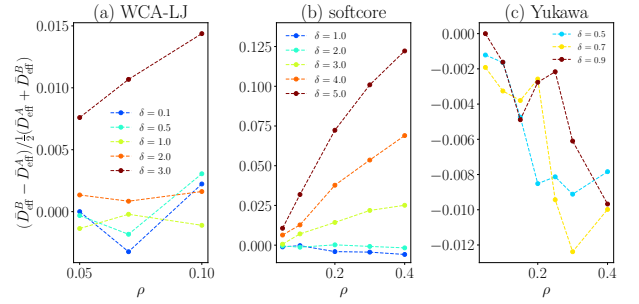


FIG. 5. Relative difference between the effective diffusion coefficient of A and B particles, for the different set of numerical simulations we performed. We show this relative difference as a function of ρ , for different values of the non-reciprocity parameter δ .

tracer (which is different from A and B in the most general situation). Finally, although the results presented in the main text applied to a three-dimensional systems, we provide here a derivation that holds in any spatial dimension d .

1. Linearized Dean equation

We start from Eq. (5). We linearize the density fields $\hat{\rho}_\alpha$ around the homogeneous value ρ_α , by writing $\hat{\rho}_\alpha = \rho_\alpha + \sqrt{\rho_\alpha} \psi_\alpha$ and assuming $\psi_\alpha \ll \sqrt{\rho_\alpha}$. We find, at

leading order in ψ_i :

$$\begin{aligned} \partial_t \psi_A &= \sqrt{2D_A} \nabla \cdot \boldsymbol{\eta}_A + D_A \nabla^2 \psi_A \\ &- \rho \mu_A [\nabla \cdot (X \mathbf{F}_{A \rightarrow A} * \psi_A) \\ &+ \nabla \cdot (\sqrt{X(1-X)} \mathbf{F}_{B \rightarrow A} * \psi_B) \\ &+ \frac{\sqrt{\rho_A}}{\rho} \nabla \cdot (\mathbf{F}_{0 \rightarrow A} * \delta_{\mathbf{r}_0})], \end{aligned} \quad (\text{D1})$$

and the counterpart for ψ_B . For simplicity, we denoted $X_A = X$ and $X_B = 1 - X$. In Fourier space, the coupled equations for $\tilde{\psi}_A(\mathbf{q}, t)$ and $\tilde{\psi}_B(\mathbf{q}, t)$ then read

$$\begin{aligned} \partial_t \begin{pmatrix} \tilde{\psi}_A(\mathbf{q}, t) \\ \tilde{\psi}_B(\mathbf{q}, t) \end{pmatrix} &= -\mathbf{m} \begin{pmatrix} \tilde{\psi}_A(\mathbf{q}, t) \\ \tilde{\psi}_B(\mathbf{q}, t) \end{pmatrix} + \begin{pmatrix} \sqrt{2D_A} i\mathbf{q} \cdot \tilde{\boldsymbol{\eta}}_A \\ \sqrt{2D_B} i\mathbf{q} \cdot \tilde{\boldsymbol{\eta}}_B \end{pmatrix} \\ &- \rho \begin{pmatrix} \sqrt{\frac{X}{\rho}} e^{-i\mathbf{q} \cdot \mathbf{r}_0(t)} \mu_A i\mathbf{q} \cdot \tilde{\mathbf{F}}_{0 \rightarrow A} \\ \sqrt{\frac{1-X}{\rho}} e^{-i\mathbf{q} \cdot \mathbf{r}_0(t)} \mu_B i\mathbf{q} \cdot \tilde{\mathbf{F}}_{0 \rightarrow B} \end{pmatrix}, \end{aligned} \quad (\text{D2})$$

with

$$\mathbf{m} = \begin{pmatrix} q^2 k_B T_A \mu_A + \rho \mu_A X i\mathbf{q} \cdot \tilde{\mathbf{F}}_{A \rightarrow A} & \\ \rho \mu_B \sqrt{X(1-X)} i\mathbf{q} \cdot \tilde{\mathbf{F}}_{A \rightarrow B} & \\ \rho \mu_A \sqrt{X(1-X)} i\mathbf{q} \cdot \tilde{\mathbf{F}}_{B \rightarrow A} & \\ q^2 k_B T_B \mu_B + \rho \mu_B (1-X) i\mathbf{q} \cdot \tilde{\mathbf{F}}_{B \rightarrow B} \end{pmatrix} \quad (\text{D3})$$

We apply the same procedure to the equation for the position of the tracer, which reads

$$\begin{aligned} \frac{d}{dt} \mathbf{r}_0(t) &= \rho \mu_0 \sqrt{\frac{X}{\rho}} (\mathbf{F}_{A \rightarrow 0} * \psi_A)(\mathbf{r}_0(t), t) \\ &+ \rho \mu_0 \sqrt{\frac{1-X}{\rho}} (\mathbf{F}_{B \rightarrow 0} * \psi_B)(\mathbf{r}_0(t), t) + \sqrt{2D_0} \boldsymbol{\xi}(t) \end{aligned} \quad (\text{D4})$$

In order to treat the coupling between the dynamics of the fields and that of the position of the tracer, we rely on a path-integral formulation, that was initially proposed in the situation where the tracer is coupled to a single fluctuating field [38], and later extended to the situation where the tracer is coupled to multiple fields [39]. In Section D 2, we present a general formalism, that applies to a tracer particle coupled in a non-reciprocal way to two fluctuating fields, which themselves interact non-reciprocally. In Section D 4, we show how the formalism can be applied to the case where the fluctuating fields represent the stochastic density fields of *A* and *B* particles.

2. General formalism

a. Dynamics of the tracer and of the fields

We consider a tracer, whose position at time t is denoted by $\mathbf{r}_0(t)$, and which diffuses while being coupled to

two fluctuating fields $\psi_A(\mathbf{x}, t)$ and $\psi_B(\mathbf{x}, t)$ (Fig. 6). We assume that the interactions between the two fields can be non-reciprocal and also that the tracer-field interactions can be non-reciprocal. The position of tracer $\mathbf{r}_0(t)$ obeys the following evolution equation:

$$\frac{d}{dt} \mathbf{r}_0(t) = \mu_0 \sum_{\alpha=A,B} \nabla K_\alpha \psi_\alpha[\mathbf{r}_0(t)] + \sqrt{2D_0} \boldsymbol{\eta}(t), \quad (\text{D5})$$

where μ_0 is the mobility of the tracer, h_α is the coupling constant between the tracer and the field α , and K_α is a linear operator. Throughout the calculation we use the following shorthand notations for convolutions between operators and fields:

$$AV(\mathbf{x}) = \int d\mathbf{x}' A(\mathbf{x} - \mathbf{x}') V(\mathbf{x}), \quad (\text{D6})$$

$$ABV(\mathbf{x}) = \int d\mathbf{x}' \int d\mathbf{x}'' A(\mathbf{x} - \mathbf{x}') B(\mathbf{x}' - \mathbf{x}'') V(\mathbf{x}''). \quad (\text{D7})$$

The noise term $\boldsymbol{\eta}(t)$ has average zero and unit variance: $\langle \eta_i(t) \eta_j(s) \rangle = \delta_{ij} \delta(t - s)$.

Dynamics of the fields.— We then assume that the fields ψ_A and ψ_B obey the following dynamics:

$$\begin{aligned} \partial_t \psi_A(\mathbf{x}, t) &= -R_A [\Delta_{AA} \psi_A + \Delta_{AB} \psi_B] \\ &+ R_A K'_A[\mathbf{x} - \mathbf{r}_0(t)] + \sqrt{2D_A} \xi_A(\mathbf{x}, t) \end{aligned} \quad (\text{D8})$$

$$\begin{aligned} \partial_t \psi_B(\mathbf{x}, t) &= -R_B [\Delta_{BA} \psi_A + \Delta_{BB} \psi_B] \\ &+ R_B K'_B[\mathbf{x} - \mathbf{r}_0(t)] + \sqrt{2D_B} \xi_B(\mathbf{x}, t) \end{aligned} \quad (\text{D9})$$

where μ_α is the mobility of the field α , R_α is an operator used to specify if the dynamics is conservative or not (in Fourier space, $\tilde{R}_\alpha(\mathbf{q}) = 1$ corresponds to a non-conserved ‘model A’ dynamics, whereas $\tilde{R}_\alpha(\mathbf{q}) = \mathbf{q}^2$ corresponds to a conserved ‘model B’ dynamics [51]). Note that, for non-reciprocal interactions, $K_\alpha \neq K'_\alpha$. The noise terms are such that $\langle \xi_\alpha(\mathbf{x}, t) \xi_\beta(\mathbf{x}', s) \rangle = \delta_{\alpha\beta} R_\alpha(\mathbf{x} - \mathbf{x}') \delta(t - s)$.

The first term in the rhs of Eqs. (D8) and (D9), describes the interactions between the fields, whereas the

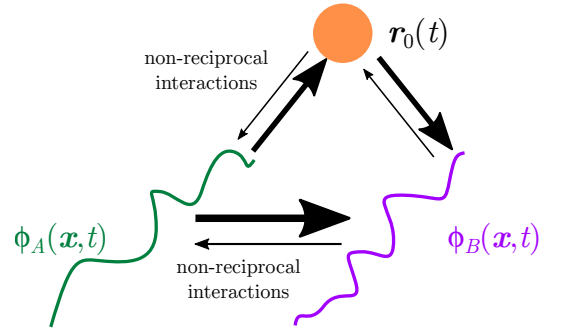


FIG. 6. A diffusing tracer is coupled to two fluctuating fields, whose interactions may be non-reciprocal. The tracer-field interactions may also be non-reciprocal.

second term describes the effect of the probe on the evolution of the fields. Note that, as opposed to the calculation proposed in [38], we do not assume that the dynamics of the system can be written as deriving from a Hamiltonian $\mathcal{H}[\mathbf{r}_0(t), \psi_A, \psi_B]$. Indeed, this choice of dynamics would yield reciprocal interactions between fields A and B , by construction.

We then follow the lines of the calculation presented in Ref. [39], and we recall all the steps for completeness. The main difference is that the tracer-bath coupling are represented differently in Eq. (D5) and in Eqs. (D8)-(D9): the reciprocal case would be recovered in the particular case $K'_A = K_A$ and $K'_B = K_B$.

b. Generalized Langevin equation for the tracer

The next step of the calculation consists in deriving a generalized Langevin equation obeyed by the position of the tracer. To this end, we first solve for the dynamics of the fields $\psi_\alpha(\mathbf{r}, t)$. We start from Eq. (D8) and (D9). The equations for ψ_A and ψ_B read, in Fourier space:

$$\frac{d}{dt} \begin{pmatrix} \tilde{\psi}_A(\mathbf{q}, t) \\ \tilde{\psi}_B(\mathbf{q}, t) \end{pmatrix} = -\mathbf{m} \begin{pmatrix} \tilde{\psi}_A \\ \tilde{\psi}_B \end{pmatrix} + \begin{pmatrix} e^{-i\mathbf{q}\cdot\mathbf{r}_0(t)} \tilde{R}_A \tilde{K}'_A + \sqrt{2D_A} \tilde{\xi}_A \\ e^{-i\mathbf{q}\cdot\mathbf{r}_0(t)} \tilde{R}_B \tilde{K}'_B + \sqrt{2D_B} \tilde{\xi}_B \end{pmatrix}, \quad (\text{D10})$$

where the dependences over \mathbf{q} are not written explicitly for clarity, and where we define the matrix \mathbf{m} as

$$\mathbf{m} = \begin{pmatrix} \tilde{R}_A \tilde{\Delta}_{AA} & \tilde{R}_A \tilde{\Delta}_{BA} \\ \tilde{R}_B \tilde{\Delta}_{AB} & \tilde{R}_B \tilde{\Delta}_{BB} \end{pmatrix}. \quad (\text{D11})$$

Eq. (D10) is a simple set of coupled linear first order differential equations, whose resolution requires the matrix exponential $\tilde{\mathcal{M}} \equiv \exp[-(t-s)\mathbf{m}]$, which is written under the form

$$\mathcal{M}_{\alpha\beta} = c_{\alpha\beta}^{(+)} e^{-(t-s)\lambda_+} + c_{\alpha\beta}^{(-)} e^{-(t-s)\lambda_-}, \quad (\text{D12})$$

where we defined the matrices

$$\mathbf{c}(\pm) = \frac{1}{2s} \begin{pmatrix} \pm m_{AA} \mp m_{BB} + s & \pm 2m_{AB} \\ \pm 2m_{BA} & \mp m_{AA} \pm m_{BB} + s \end{pmatrix}, \quad (\text{D13})$$

the eigenvalues

$$\lambda_{\pm} = \frac{m_{AA} + m_{BB}}{2} \pm \frac{1}{2} \sqrt{(m_{AA} - m_{BB})^2 + 4m_{AB}m_{BA}}, \quad (\text{D14})$$

and the quantity

$$s = \sqrt{(m_{AA} - m_{BB})^2 + 4m_{AB}m_{BA}}. \quad (\text{D15})$$

After Fourier inversion, one finds the solution of Eq. (D8) in real space under the form

$$\psi_\alpha(\mathbf{x}, t) = \int_{-\infty}^t ds \sum_{\beta} \left\{ \mathcal{M}_{\alpha\beta}(t-s) R_\beta K'_\beta[\mathbf{x} - \mathbf{r}_0(s)] + \sqrt{2D_\beta} \mathcal{M}_{\alpha\beta}(t-s) \xi_\alpha(\mathbf{x}, s) \right\}, \quad (\text{D16})$$

where $\mathcal{M}_{\alpha\beta}$ are the elements of the inverse Fourier transform of $\tilde{\mathcal{M}}$.

Starting from Eq. (D5) and using the expression for the field derived previously [Eq. (D16)], the equation for the dynamics of the tracer can be rewritten as

$$\frac{d}{dt} \mathbf{r}_0(t) = \sqrt{2D_0} \boldsymbol{\eta}(t) + \int_{-\infty}^t ds \mathbf{F}[\mathbf{r}_0(t) - \mathbf{r}_0(s), t-s] + \boldsymbol{\Xi}[\mathbf{x}_0(t), t], \quad (\text{D17})$$

with

$$\mathbf{F}(\mathbf{r}, t) = \mu_0 \sum_{\alpha, \beta} \nabla K_\alpha \mathcal{M}_{\alpha\beta}(t) R_\beta K'_\beta(\mathbf{r}), \quad (\text{D18})$$

and

$$\boldsymbol{\Xi}[\mathbf{r}, t] = \mu_0 \sum_{\alpha, \beta} \sqrt{2D_\beta} \nabla K_\alpha \int_{-\infty}^t ds \mathcal{M}_{\alpha\beta}(t-s) \xi_\beta(\mathbf{r}, s) \quad (\text{D19})$$

Therefore, the dynamics of the tracer [Eq. (D17)] is formally written as a generalized Langevin equation.

c. Path-integral representation

Starting from Eq. (D17), we now aim at calculating the mean-square displacement of the tracer at a given time t_f , defined as $\langle [\mathbf{r}_0(t_f) - \mathbf{r}_0(0)]^2 \rangle$, and the self-diffusion coefficient, defined as

$$D_{\text{eff}} = \lim_{t_f \rightarrow \infty} \frac{\langle [\mathbf{r}_0(t_f) - \mathbf{r}_0(0)]^2 \rangle}{2t_f} \quad (\text{D20})$$

To this end, we follow the lines of Ref. [38], in which a perturbative path-integral study was outlined. Introducing a variable \mathbf{p} conjugated to the position of the tracer, the partition function associated to Eq. (D17) can be written under the form $Z = \int \mathcal{D}\mathbf{x} \mathcal{D}\mathbf{p} e^{-S[\mathbf{x}, \mathbf{p}]}$, where the action $S[\mathbf{x}, \mathbf{p}] = S_0[\mathbf{x}, \mathbf{p}] + S_{\text{int}}[\mathbf{x}, \mathbf{p}]$ has the following contributions:

$$S_0[\mathbf{x}, \mathbf{p}] = -i \int dt p_i(t) \dot{x}_i(t) + D_0 \int dt p_i(t) p_i(t), \quad (\text{D21})$$

$$S_{\text{int}}[\mathbf{x}, \mathbf{p}] = i \int dt ds p_i(t) F_i[\mathbf{r}_0(t) - \mathbf{r}_0(s), t-s] \theta(t-s) + \int dt ds p_i(t) G_{ij}[\mathbf{r}_0(t) - \mathbf{r}_0(s), t-s] p_j(t) \theta(t-s). \quad (\text{D22})$$

We used the Einstein summation convention and where θ denotes the Heaviside function. The matrix elements G_{ij} are defined as $G_{ij}(\mathbf{x} - \mathbf{x}', t - t') \equiv \langle \Xi_i(\mathbf{x}, t) \Xi_j(\mathbf{x}', t') \rangle$, and read, in Fourier space:

$$\tilde{G}_{ij}(\mathbf{q}, t) = 2\mu_0^2 q_i q_j \sum_{\alpha, \beta, \gamma} \tilde{K}_\alpha \tilde{K}_\gamma k_B T_\beta \tilde{R}_\beta \times \sum_{\nu, \epsilon = \pm 1} c_{\alpha\beta}^{(\nu)} c_{\gamma\beta}^{(\epsilon)} \frac{e^{-\lambda_\nu |t|}}{\lambda_\nu + \lambda_\epsilon}, \quad (\text{D23})$$

where the sums over α , β and γ run over all the constituents of the mixture, and where we use the expression of the matrix exponential $\mathcal{M}_{\alpha\beta}$ given in Eq. (D12). Similarly, the Fourier transform of the components of \mathbf{F} , defined in Eq. (D18), read

$$\tilde{F}_i(\mathbf{q}, t) = i\mu_0 \mathbf{q} \sum_{\alpha\beta} \tilde{K}_\alpha \tilde{\mathcal{M}}_{\alpha\beta}(t) \tilde{R}_\beta \tilde{K}'_\beta. \quad (\text{D24})$$

At equilibrium, when $\tilde{K}_\alpha = K'_\alpha$, $T_\alpha = T$ and $\Delta_{\alpha\beta} = \Delta_{\beta\alpha}$, one can check that the functions \mathbf{F} and \mathbf{G} satisfy the relation $\nabla_i F_j(\mathbf{x}, t) = \partial_t G_{ij}(\mathbf{x}, t)$ for $t > 0$ [52].

Expanding in the limit where the tracer-bath interactions are small (i.e. when the interaction action S_{int} is small compared to S_0) and at first nontrivial order, one gets the following expression for the mean-square displacement of the tracer:

$$\langle [\mathbf{r}_0(t_f) - \mathbf{r}_0(0)]^2 \rangle \simeq \langle [\mathbf{r}_0(t_f) - \mathbf{r}_0(0)]^2 \rangle_0 - I_F - I_G, \quad (\text{D25})$$

where the average $\langle \dots \rangle_0$ is taken over the bare action S_0 , and where we defined

$$I_F = \left\langle i \mathbf{r}_0(t_f)^2 \int dt \int ds \theta(t-s) p_i(t) \times F_i[\mathbf{r}_0(t) - \mathbf{r}_0(s), t-s] \right\rangle_0 \quad (\text{D26})$$

$$\begin{aligned} t_f \xrightarrow{\simeq} \infty 4D_0 \int \frac{d^d \mathbf{q}}{(2\pi)^d} q^2 \mu_0 \sum_{\alpha,\beta} \tilde{K}_\alpha(\mathbf{q}) \tilde{K}'_\beta(\mathbf{q}) \tilde{R}_\beta(\mathbf{q}) \\ \times \sum_{\nu=\pm 1} \frac{c_{\alpha\beta}^{(\nu)}}{(D_0 q^2 + \lambda_\nu)^2} t_f, \end{aligned} \quad (\text{D27})$$

and

$$I_G = \left\langle \mathbf{r}_0(t_f)^2 \int dt \int ds \theta(t-s) p_i(t) \times G_{ij}[\mathbf{r}_0(t) - \mathbf{r}_0(s), t-s] p_j(s) \right\rangle_0 \quad (\text{D28})$$

$$\begin{aligned} t_f \xrightarrow{\simeq} \infty 4 \int \frac{d^d \mathbf{q}}{(2\pi)^d} q^2 \mu_0^2 \sum_{\alpha,\beta,\gamma} \tilde{K}_\alpha(\mathbf{q}) \tilde{K}_\gamma(\mathbf{q}) \tilde{R}_\beta(\mathbf{q}) k_B T_\beta \\ \times \sum_{\nu,\epsilon=\pm 1} \frac{c_{\alpha,\beta}^{(\nu)} c_{\gamma,\beta}^{(\epsilon)}}{\lambda_\nu + \lambda_\epsilon} \cdot \frac{D_0 q^2 - \lambda_\nu}{(D_0 q^2 + \lambda_\nu)^2} t_f. \end{aligned} \quad (\text{D29})$$

Then, using the definition of the effective diffusion coefficient and integrating over all Fourier modes, we write the effective diffusion coefficient under the form

$D_{\text{eff}} = D_0 - \sum_{\alpha,\beta} \bar{D}_{\alpha\beta}$ with

$$\begin{aligned} \bar{D}_{\alpha\beta} &= \frac{\mu_0}{d} \int \frac{d^d \mathbf{q}}{(2\pi)^d} q^2 \tilde{K}_\alpha(\mathbf{q}) \tilde{R}_\beta(\mathbf{q}) \\ &\times \sum_\gamma \sum_{\nu=\pm 1} \frac{c_{\alpha\beta}^{(\nu)}}{(D_0 q^2 + \lambda_\nu)^2} \left[2D_0 \delta_{\gamma\beta} \tilde{K}'_\gamma(\mathbf{q}) \right. \\ &\left. + D_0 \left(\frac{c_{\gamma\beta}^{(\nu)}}{\lambda_\nu} + \frac{2c_{\gamma\beta}^{(-\nu)}}{\lambda_+ + \lambda_-} \right) (D_0 q^2 - \lambda_\nu) \tilde{K}_\gamma(\mathbf{q}) \right]. \end{aligned} \quad (\text{D30})$$

3. Correction to the mobility

Here we adapt the calculation above to the correction to the mobility, following Ref. [34]. We apply a small external force \mathbf{f} and compute the correction to the average tracer position, $\langle \mathbf{r}_0(t_f) - \mathbf{r}_0(0) \rangle$. The bare action is now given by

$$\begin{aligned} S_0[\mathbf{x}, \mathbf{p}] &= -i \int dt p_i(t) [\dot{r}_{0,i}(t) - \mu_0 \mathbf{f}] \\ &+ D_0 \int dt p_i(t) p_i(t), \end{aligned} \quad (\text{D31})$$

The average displacement of the tracer is

$$\langle \mathbf{r}_0(t_f) - \mathbf{r}_0(0) \rangle = \mu_0 \mathbf{f} t_f - I'_F - I'_G, \quad (\text{D32})$$

where the following averages are computed with Ref. [34] (Eqs. (72, 73)):

$$\begin{aligned} I'_F &= \left\langle i \mathbf{r}_0(t_f) \int dt \int ds \theta(t-s) p_i(t) \right. \\ &\left. \times F_i[\mathbf{r}_0(t) - \mathbf{r}_0(s), t-s] \right\rangle_0 \end{aligned} \quad (\text{D33})$$

$$\begin{aligned} &= -i\mu_0 t_f \int \frac{d^d \mathbf{q}}{(2\pi)^d} \sum_{\alpha,\beta} \sum_{\nu=\pm 1} \frac{\mathbf{q} \tilde{K}_\alpha \tilde{K}'_\beta \tilde{R}_\beta c_{\alpha\beta}^{(\nu)}}{\lambda_\nu + D_0 q^2 - i\mu_0 \mathbf{q} \cdot \mathbf{f}}. \end{aligned} \quad (\text{D34})$$

and

$$\begin{aligned} I'_G &= \left\langle \mathbf{r}_0(t_f) \int dt \int ds \theta(t-s) p_i(t) \right. \\ &\left. \times G_{ij}[\mathbf{r}_0(t) - \mathbf{r}_0(s), t-s] p_j(s) \right\rangle_0 \end{aligned} \quad (\text{D35})$$

$$\begin{aligned} &= -2i\mu_0^2 t_f \int \frac{d^d \mathbf{q}}{(2\pi)^d} \sum_{\alpha,\beta,\gamma} \sum_{\nu,\epsilon=\pm 1} \mathbf{q} q^2 \tilde{K}_\alpha \tilde{K}_\gamma k_B T_\beta \tilde{R}_\beta \\ &\times \frac{c_{\alpha\beta}^{(\nu)} c_{\gamma\beta}^{(\epsilon)}}{(\lambda_\nu + \lambda_\epsilon)(\lambda_\nu + D_0 q^2 - i\mu_0 \mathbf{q} \cdot \mathbf{f})}. \end{aligned} \quad (\text{D36})$$

To obtain the effective mobility, we take the limit $f \rightarrow 0$ and consider the velocity in the direction of the force,

leading to

$$\begin{aligned} \mu_{\text{eff}} &= \mu_0 - \frac{\mu_0^2}{d} \int \frac{d^d \mathbf{q}}{(2\pi)^d} \sum_{\alpha, \beta} \sum_{\nu = \pm 1} \frac{q^2 \tilde{K}_\alpha \tilde{K}'_\beta \tilde{R}_\beta c_{\alpha\beta}^{(\nu)}}{(\lambda_\nu + D_0 q^2)^2} \\ &\quad - \frac{2\mu_0^3}{d} \int \frac{d^d \mathbf{q}}{(2\pi)^d} \sum_{\alpha, \beta, \gamma} \sum_{\nu, \epsilon = \pm 1} \frac{q^4 \tilde{K}_\alpha \tilde{K}_\gamma k_B T_\beta \tilde{R}_\beta c_{\alpha\beta}^{(\nu)} c_{\gamma\beta}^{(\epsilon)}}{(\lambda_\nu + \lambda_\epsilon)(\lambda_\nu + D_0 q^2)^2} \end{aligned} \quad (\text{D37})$$

$$\begin{aligned} &= \mu_0 - \frac{\mu_0^2}{d} \int \frac{d^d \mathbf{q}}{(2\pi)^d} \sum_{\alpha, \beta} \sum_{\nu = \pm 1} \frac{q^2 \tilde{K}_\alpha \tilde{R}_\beta c_{\alpha\beta}^{(\nu)}}{(\lambda_\nu + D_0 q^2)^2} \\ &\quad \times \left[\tilde{K}'_\beta + 2\mu_0 k_B T_\beta q^2 \sum_{\gamma} \sum_{\epsilon = \pm 1} \frac{\tilde{K}_\gamma c_{\gamma\beta}^{(\epsilon)}}{\lambda_\nu + \lambda_\epsilon} \right]. \end{aligned} \quad (\text{D38})$$

4. Mapping with the situation considered in the main text

The equations of the main text, which were derived in the specific situations where the fields ψ_A and ψ_B describe the perturbation around homogeneous densities of interacting Brownian particles, are mapped onto the general equations [Eqs. (D5) and (D10)] using the following expressions for the operators R_α , $\Delta_{\alpha\beta}$, K_α and K'_α :

$$\tilde{R}_\alpha(\mathbf{q}) = \mu_\alpha q^2 \quad (\text{D39})$$

$$\begin{cases} \tilde{\Delta}_{AA} = k_B T_A q^2 + \rho X \mathbf{iq} \cdot \tilde{\mathbf{F}}_{A \rightarrow A} \\ \tilde{\Delta}_{BB} = k_B T_B q^2 + \rho(1-X) \mathbf{iq} \cdot \tilde{\mathbf{F}}_{B \rightarrow B} \\ \tilde{\Delta}_{AB} = \rho \sqrt{X(1-X)} \mathbf{iq} \cdot \tilde{\mathbf{F}}_{B \rightarrow A} \\ \tilde{\Delta}_{BA} = \rho \sqrt{X(1-X)} \mathbf{iq} \cdot \tilde{\mathbf{F}}_{A \rightarrow B} \end{cases} \quad (\text{D40})$$

$$\begin{cases} \tilde{K}_A = -\frac{\sqrt{\rho X}}{q^2} \mathbf{iq} \cdot \tilde{\mathbf{F}}_{A \rightarrow 0} \\ \tilde{K}_B = -\frac{\sqrt{\rho(1-X)}}{q^2} \mathbf{iq} \cdot \tilde{\mathbf{F}}_{B \rightarrow 0} \end{cases} \quad (\text{D41})$$

$$\neq \begin{cases} \tilde{K}'_A = -\frac{\sqrt{\rho X}}{q^2} \mathbf{iq} \cdot \tilde{\mathbf{F}}_{0 \rightarrow A} \\ \tilde{K}'_B = -\frac{\sqrt{\rho(1-X)}}{q^2} \mathbf{iq} \cdot \tilde{\mathbf{F}}_{0 \rightarrow B} \end{cases}. \quad (\text{D42})$$

5. Expression of the long-time diffusion coefficient and mobility

Using the mapping from Eqs. (D39)-(D42), we get the following expression of the effective diffusion coefficient of the tracer particle:

$$\begin{aligned} \frac{D_{\text{eff}}}{D_0} &= 1 - \sum_{\alpha, \beta, \gamma} \mu_0 \mu_\beta \int_0^\infty \frac{dq}{6\pi^2} q^2 \rho \sqrt{X_\alpha X_\gamma} \mathbf{iq} \cdot \tilde{\mathbf{F}}_{\alpha \rightarrow 0} \\ &\quad \times \sum_{\nu = \pm 1} \frac{2c_{\alpha\beta}^{(\nu)}}{(D_0 q^2 + \lambda_\nu)^2} \left[\delta_{\gamma\beta} \mathbf{iq} \cdot \tilde{\mathbf{F}}_{0 \rightarrow \gamma} \right. \\ &\quad \left. + \frac{T_\beta}{T_0} (D_0 q^2 - \lambda_\nu) \sum_{\epsilon = \pm 1} \frac{c_{\gamma\beta}^{(\epsilon)}}{\lambda_\nu + \lambda_\epsilon} \mathbf{iq} \cdot \tilde{\mathbf{F}}_{\gamma \rightarrow 0} \right], \end{aligned} \quad (\text{D43})$$

where $\lambda_{\pm 1}$ denote the eigenvalues of \mathbf{m} , and where the coefficients $c_{\alpha\beta}^{(\pm 1)}$ are the elements of the matrices

$$\mathbf{c}^{(\pm)} = \frac{1}{2s} \begin{pmatrix} \pm m_{AA} \mp m_{BB} + s & \pm 2m_{AB} \\ \pm 2m_{BA} & \mp m_{AA} \pm m_{BB} + s \end{pmatrix}, \quad (\text{D44})$$

with

$$\begin{aligned} s &\equiv \{ [(q^2 k_B T_A \mu_A + \rho \mu_A X \mathbf{iq} \cdot \mathbf{F}_{A \rightarrow A}) \\ &\quad - (q^2 k_B T_B \mu_B + \rho \mu_B (1-X) \mathbf{iq} \cdot \mathbf{F}_{B \rightarrow B})]^2 \\ &\quad + 4\rho^2 \mu_A \mu_B X(1-X) (\mathbf{iq} \cdot \mathbf{F}_{A \rightarrow B}) (\mathbf{iq} \cdot \mathbf{F}_{B \rightarrow A}) \}^{1/2}. \end{aligned} \quad (\text{D45})$$

The expression given of D_{eff}/D_0 in the main text [Eq. (6)] is obtained by considering the simple case where all the particles have the same mobilities, the same diffusion coefficients, and are connected to the same thermostat. We also consider the particular case where the forces derive from pseudo-potentials, i.e. in Fourier space:

$$\mathbf{F}_{\alpha \rightarrow \beta}(\mathbf{q}) = -\mathbf{iq} \tilde{\phi}_{\alpha \rightarrow \beta}(\mathbf{q}). \quad (\text{D46})$$

This yields the expression from the main text:

$$\begin{aligned} \frac{D_{\text{eff}}}{D_0} &= 1 - \sum_{\substack{\alpha, \beta, \gamma \\ \in \{A, B\}}} \int \frac{dq}{6\pi^2} \rho q^2 \tilde{\phi}_{\alpha \rightarrow 0}(q) \\ &\quad \times \sum_{\gamma} \sqrt{X_\alpha X_\gamma} \left[C_{0 \rightarrow \gamma}^{\alpha\beta\gamma} \tilde{\phi}_{\alpha \rightarrow 0}(q) + C_{\gamma \rightarrow 0}^{\alpha\beta\gamma} \tilde{\phi}_{\gamma \rightarrow 0}(q) \right], \end{aligned} \quad (\text{D47})$$

with

$$C_{0 \rightarrow \gamma}^{\alpha\beta\gamma} = \delta_{\gamma\beta} \sum_{\nu = \pm 1} \frac{2c_{\alpha\beta}^{(\nu)}}{(1 + \bar{\lambda}_\nu)^2}, \quad (\text{D48})$$

$$C_{\gamma \rightarrow 0}^{\alpha\beta\gamma} = \sum_{\nu, \epsilon = \pm 1} \frac{2c_{\alpha\beta}^{(\nu)} c_{\gamma\beta}^{(\epsilon)}}{(1 + \bar{\lambda}_\nu)^2 (\bar{\lambda}_\nu + \bar{\lambda}_\epsilon)} (1 - \bar{\lambda}_\nu), \quad (\text{D49})$$

where we defined $\bar{\lambda}_\nu = \lambda_\nu / (D_0 q^2)$.

Similarly, using the mapping and the expression of the mobility [Eq. (D38)], we get

$$\begin{aligned} \frac{\mu_{\text{eff}}}{D_0} &= 1 - \sum_{\alpha, \beta, \gamma} \mu_0 \int_0^\infty \frac{dq}{6\pi^2} q^2 \rho \sqrt{X_\alpha X_\gamma} \mathbf{iq} \cdot \tilde{\mathbf{F}}_{\alpha \rightarrow 0} \\ &\quad \times \sum_{\nu = \pm 1} \frac{c_{\alpha\beta}^{(\nu)}}{(D_0 q^2 + \lambda_\nu)^2} \left[\delta_{\gamma\beta} \mathbf{iq} \cdot \tilde{\mathbf{F}}_{0 \rightarrow \gamma} \right. \\ &\quad \left. + 2\mu_0 k_B T_\beta q^2 \sum_{\epsilon = \pm 1} \frac{c_{\gamma\beta}^{(\epsilon)}}{\lambda_\nu + \lambda_\epsilon} \mathbf{iq} \cdot \tilde{\mathbf{F}}_{\gamma \rightarrow 0} \right]. \end{aligned} \quad (\text{D50})$$

Appendix E: Effective mobility of a probe coupled non-reciprocally to a single bath

In this section, we explain the derivation of the effective mobility of a probe coupled non-reciprocally to a

single bath (see Eq. (8) in the main text). We rely on the derivation presented in [40], in which the mean displacement of a probe linearly coupled to a generic fluctuating field, and submitted to a driven harmonic confinement, is computed. In Eq. (A.3) from this reference, the terms in brackets in the integrand has two contributions: the first one originates from memory effects, and should be proportional to the effect of the bath on the tracer times that of the tracer on the bath; the second one originates from the noise of the bath, and should be proportional to the square of the effect of the bath on the tracer.

Denoting by $(1 - \delta)$ the effect of the bath on the tracer, as in the main text, and taking the limit of a harmonic trap of vanishing stiffness and vanishing velocity, we find from Eq. (A.3) in [40]:

$$\mu_{\text{eff}} = \mu_0 - \frac{1}{3} \int \frac{d\mathbf{q}}{(2\pi)^3} \frac{q^2 \tilde{K}^2}{\tilde{A}} \frac{(1 - \delta)((1 - \delta)D_0 q^2 + \tilde{R}\tilde{A})}{(D_0 q^2 + \tilde{R}\tilde{A})^2}, \quad (\text{E1})$$

Using the following mapping between the notations of [40] and our notations: $\tilde{K}^2 = \rho\tilde{v}^2$, $\tilde{A} = 1 + \rho\tilde{v}$, $\tilde{R} = \mu_0 q^2$, we find the result given in the main text. This expression can also be obtained as a consequence of the more general expression of the long-time mobility [Eq. (D38)].

Appendix F: Low-density limit

1. Friction

In order to measure the friction of the tracer particle in the low-density limit, we assume that it is submitted to a small external force, along the lines of [41]. Applying a force \mathbf{F} on the probe disturbs the pair distribution function $g_{\alpha\beta}(\mathbf{r})$, which is now a solution of

$$0 = 2D_0 \nabla \cdot [e^{-u_{\alpha\beta}} \nabla (e^{u_{\alpha\beta}} g_{\alpha\beta})] + \mu_0 \mathbf{F} \cdot \nabla g_{\alpha\beta}, \quad (\text{F1})$$

where we recall the definition of $u_{\alpha\beta}$ given in the main text: $u_{\alpha\beta}(r) = [\phi_{\alpha \rightarrow \beta}(r) + \phi_{\beta \rightarrow \alpha}(r)]/2k_B T$. We use the ansatz

$$g_{\alpha\beta}(\mathbf{r}) = g_{\alpha\beta}^0(r) [1 + q(r) \mathbf{F} \cdot \hat{\mathbf{r}}], \quad (\text{F2})$$

where $g_{\alpha\beta}^0(r)$ is the pair distribution function in the absence of external force. In the limit of small force, the first order in $\mathbf{F} = F \hat{\mathbf{F}}$ reads

$$0 = 2D_0 \nabla \cdot [e^{-u_{\alpha\beta}(r)} \nabla (q(r) \hat{\mathbf{F}} \cdot \hat{\mathbf{r}})] + \mu_0 \hat{\mathbf{F}} \cdot \nabla e^{-u_{\alpha\beta}(r)}. \quad (\text{F3})$$

Writing explicitly the derivative and using $D_0 = k_B T \mu_0$, we get

$$2\nabla \cdot [e^{-u_{\alpha\beta}(r)} \nabla (q(r) \hat{\mathbf{F}} \cdot \hat{\mathbf{r}})] = \frac{1}{k_B T} \hat{\mathbf{F}} \cdot \hat{\mathbf{r}} u'_{\alpha\beta}(r) e^{-u_{\alpha\beta}(r)}. \quad (\text{F4})$$

The friction created by the bath particles is

$$\mathbf{F}_b = \sum_{\beta} \rho_{\beta} \int g_{\alpha\beta}(\mathbf{r}) \nabla \phi_{\beta \rightarrow \alpha}(r) d\mathbf{r}. \quad (\text{F5})$$

Using the ansatz (F2) leads to

$$\mathbf{F}_b = \sum_{\beta} \rho_{\beta} \int e^{-u_{\alpha\beta}(r)} q(r) (\mathbf{F} \cdot \hat{\mathbf{r}}) \hat{\mathbf{r}} \phi'_{\beta \rightarrow \alpha}(r) d\mathbf{r} \quad (\text{F6})$$

$$= \sum_{\beta} \frac{\rho_{\beta}}{3} \mathbf{F} \int e^{-u_{\alpha\beta}(r)} q(r) \phi'_{\beta \rightarrow \alpha}(r) d\mathbf{r} \quad (\text{F7})$$

The relative change in mobility is thus

$$\frac{\mu_{\text{eff}} - \mu_0}{\mu_0} = \sum_{\beta} \frac{\rho_{\beta}}{3} \int e^{-u_{\alpha\beta}(r)} q(r) \phi'_{\beta \rightarrow \alpha}(r) d\mathbf{r}. \quad (\text{F8})$$

2. Long-time diffusion coefficient

From Eq. (S21) in Ref. [42], the correction to the long time diffusion coefficient of the probe is given by

$$\Delta D = - \lim_{s \rightarrow 0} \lim_{k \rightarrow 0} \langle e^{-i\mathbf{q} \cdot \mathbf{r}_1} \mathcal{L}_N (s - \mathcal{L}_N)^{-1} \mathcal{L}_N e^{i\mathbf{q} \cdot \mathbf{r}_1} \rangle_{\text{ss}}. \quad (\text{F9})$$

The average is defined by $\langle f \rangle_{\text{ss}} = \int f(\mathbf{X}) P_N(\mathbf{X}) d\mathbf{X}$ where \mathbf{X} is the vector containing the coordinates of all the particles and $P_N(\mathbf{X})$ is the steady state probability density: $\mathcal{L}_N P_N = 0$. The Liouville operator is given by

$$\mathcal{L}_N f(\mathbf{X}) = D_0 \sum_{n=1}^N \nabla_{\mathbf{r}_n} \cdot \left[\nabla_{\mathbf{r}_n} f + f \sum_{m \neq n} \nabla_{\mathbf{r}_n} \phi_{S(m) \rightarrow S(n)}(\mathbf{r}_n - \mathbf{r}_m) \right]. \quad (\text{F10})$$

We now compute $\mathcal{L}_N e^{i\mathbf{q} \cdot \mathbf{r}_1} P_N(\mathbf{X})$. First, as $\mathcal{L}_N P_N = 0$, at least one derivative should act on $e^{i\mathbf{q} \cdot \mathbf{r}_1}$. Second, as the limit $k \rightarrow 0$ will be taken, at most one derivative should act on $e^{i\mathbf{q} \cdot \mathbf{r}_1}$. We are left with

$$\begin{aligned} \mathcal{L}_N e^{i\mathbf{q} \cdot \mathbf{r}_1} P_N(\mathbf{X}) &= D_0 e^{i\mathbf{q} \cdot \mathbf{r}_1} i\mathbf{q} \cdot \left[2\nabla_{\mathbf{r}_1} P_N(\mathbf{X}) \right. \\ &\quad \left. + P_N(\mathbf{X}) \nabla_{\mathbf{r}_1} \sum_{m \neq 1} \phi_{S(m) \rightarrow S(1)}(\mathbf{r}_1 - \mathbf{r}_m) \right]. \end{aligned} \quad (\text{F11})$$

To simplify, we consider only two particles; we will multiply by the density afterwards. We also take $P_N(\mathbf{X}) = g_{\alpha\beta}^0(\mathbf{r}_1 - \mathbf{r}_2) = \exp(-u_{\alpha\beta}(\mathbf{r}_1 - \mathbf{r}_2))$, leading to

$$\begin{aligned} \mathcal{L}_N e^{i\mathbf{q} \cdot \mathbf{r}_1} P_N(\mathbf{X}) &= -D_0 e^{i\mathbf{q} \cdot \mathbf{r}_1 - u_{\alpha\beta}(\mathbf{r}_1 - \mathbf{r}_2)} i\mathbf{q} \cdot [2\nabla_{\mathbf{r}_1} u_{\alpha\beta}(\mathbf{r}_1 - \mathbf{r}_2) \\ &\quad - \nabla_{\mathbf{r}_1} \phi_{\beta\alpha}(\mathbf{r}_1 - \mathbf{r}_2)] \end{aligned} \quad (\text{F12})$$

$$= -D_0 e^{i\mathbf{q} \cdot \mathbf{r}_1 - u_{\alpha\beta}(\mathbf{r})} i\mathbf{q} \cdot \nabla_{\mathbf{r}} [2u_{\alpha\beta}(\mathbf{r}) - \phi_{\beta\alpha}(\mathbf{r})] \quad (\text{F13})$$

$$= -D_0 e^{i\mathbf{q} \cdot \mathbf{r}_1 - u_{\alpha\beta}(\mathbf{r})} i\mathbf{q} \cdot \hat{\mathbf{r}} \phi'_{\alpha\beta}(r), \quad (\text{F14})$$

where $\mathbf{r} = \mathbf{r}_1 - \mathbf{r}_2$. Integrating by parts on the left in Eq. (F9) and taking the limit $k \rightarrow 0$ leads to

$$\Delta D = - \sum_{\beta} \mu_0^2 \rho_{\beta} I_{\alpha\beta} \quad (\text{F15})$$

with

$$I_{\alpha\beta} = \lim_{s \rightarrow 0} \int (\hat{\mathbf{q}} \cdot \hat{\mathbf{r}}) \phi'_{\beta \rightarrow \alpha}(r) (s - \mathcal{L}_{\alpha\beta})^{-1} \times g_{\alpha\beta}^0(r) \phi'_{\alpha \rightarrow \beta}(r) (\hat{\mathbf{q}} \cdot \hat{\mathbf{r}}) d\mathbf{r}. \quad (\text{F16})$$

We introduce

$$\chi_{\alpha\beta}(\mathbf{r}, t = 0) = g_{\alpha\beta}^0(r) \phi'_{\alpha \rightarrow \beta}(r) (\hat{\mathbf{q}} \cdot \hat{\mathbf{r}}), \quad (\text{F17})$$

so that

$$\lim_{s \rightarrow 0} (s - \mathcal{L}_{\alpha\beta})^{-1} \chi_{\alpha\beta}(\mathbf{r}, t = 0) = \tilde{\chi}_{\alpha\beta}(\mathbf{r}, s = 0). \quad (\text{F18})$$

The Laplace transform is solution of

$$\begin{aligned} \mathcal{L}_{\mathbf{r}} \tilde{\chi}_{\alpha\beta}(\mathbf{r}, s = 0) &= -\chi_{\alpha\beta}(\mathbf{r}, t = 0) \\ &= -e^{-u_{\alpha\beta}(r)} \phi'_{\alpha \rightarrow \beta}(r) (\hat{\mathbf{q}} \cdot \hat{\mathbf{r}}). \end{aligned} \quad (\text{F19})$$

Taking the ansatz

$$\tilde{\chi}_{\alpha\beta}(\mathbf{r}, s = 0) = g_{\alpha\beta}^0(r) X_{\alpha\beta}(r) \hat{\mathbf{q}} \cdot \hat{\mathbf{r}}, \quad (\text{F20})$$

$X_{\alpha\beta}(r)$ is the solution of

$$\begin{aligned} 2\nabla \cdot \left[e^{-u_{\alpha\beta}(r)} \nabla_r (X_{\alpha\beta}(r) \hat{\mathbf{q}} \cdot \hat{\mathbf{r}}) \right] \\ = -D_0^{-1} e^{-u_{\alpha\beta}(r)} \phi'_{\alpha \rightarrow \beta}(r) (\hat{\mathbf{q}} \cdot \hat{\mathbf{r}}). \end{aligned} \quad (\text{F21})$$

Plugging the ansatz (F20) in the correction, we get

$$I_{\alpha\beta} = \frac{1}{3} \int \phi'_{\beta \rightarrow \alpha}(r) e^{-u_{\alpha\beta}(r)} X_{\alpha\beta}(r) d\mathbf{r}, \quad (\text{F22})$$

so that finally

$$\frac{D_{\text{eff}} - D_0}{D_0} = - \sum_{\beta} \frac{\mu_0 \rho_{\beta}}{3k_{\text{B}}T} \int \phi'_{\beta \rightarrow \alpha}(r) e^{-u_{\alpha\beta}(r)} X_{\alpha\beta}(r) d\mathbf{r}. \quad (\text{F23})$$

Finally, defining $Y_{\alpha\beta} = -\mu_0 X_{\alpha\beta}/k_{\text{B}}T$, the correction and the definition of $Y_{\alpha\beta}(r)$ read

$$\frac{D_{\text{eff}} - D_0}{D_0} = \sum_{\beta} \frac{\rho_{\beta}}{3} \int \phi'_{\beta \rightarrow \alpha}(r) e^{-u_{\alpha\beta}(r)} Y_{\alpha\beta}(r) d\mathbf{r}, \quad (\text{F24})$$

and

$$2\nabla \cdot \left[e^{-u_{\alpha\beta}(r)} \nabla_r (Y_{\alpha\beta}(r) \hat{\mathbf{q}} \cdot \hat{\mathbf{r}}) \right] = \frac{1}{k_{\text{B}}T} \hat{\mathbf{q}} \cdot \hat{\mathbf{r}} \phi'_{\alpha\beta}(r) e^{-u_{\alpha\beta}(r)}. \quad (\text{F25})$$

We note that Eqs. (F25, F24) are analogous to Eqs. (F4, F8) for the effective mobility, the only change being that $u'_{\alpha\beta}(r)$ in the r.h.s of Eq. (F4) is replaced by $\phi'_{\alpha\beta}(r)$ in Eq. (F25). At equilibrium, $\phi_{\beta\alpha} = u_{\alpha\beta}$ and the Einstein relation is recovered.

3. Numerical evaluation of the correction

Equations (F4) and (F25) defining $q(r)$ and $Y_{\alpha\beta}(r)$ cannot be integrated analytically in general. We rewrite the equations here in a dimensionless form. The correction to the correlation satisfies

$$\nabla \cdot \left[e^{-u(r)} \nabla (q(r) \mathbf{n} \cdot \hat{\mathbf{r}}) \right] = \mathbf{n} \cdot \hat{\mathbf{r}} v'(r) e^{-u(r)}, \quad (\text{F26})$$

where $u(r) = u_{\alpha\beta}(r)$ and $v(r) = u_{\alpha\beta}(r)$ for the mobility and $v(r) = \phi_{\alpha\beta}(r)$ for the diffusion coefficient; the vector \mathbf{n} is arbitrary. In arbitrary dimension d , expanding this equation leads to

$$q'' + \left(\frac{d-1}{r} - u' \right) q' - \frac{d-1}{r^2} q = v'. \quad (\text{F27})$$

The correction to the quantity A ($A = \mu$ or $A = D$, depending on the function $v(r)$ used to compute $q(r)$) is then given by

$$\frac{\Delta A}{A} = \frac{S_{d-1} \bar{\rho}_{\beta}}{2d} \int_0^{\infty} e^{-u(r)} w'(r) q(r) r^{d-1} dr, \quad (\text{F28})$$

where $w(r) = \phi_{\beta\alpha}(r)$, and S_d denotes the surface of the d -dimensional unit sphere.

Instead of solving for $q(r)$, we introduce $p = qe^{-u}$, which is the solution of

$$p'' + \left(\frac{d-1}{r} + u' \right) p' + \left(u'' + \frac{d-1}{r} u' - \frac{d-1}{r^2} \right) p = v' e^{-u}. \quad (\text{F29})$$

With p , the correction reads

$$\frac{\Delta A}{A} = \frac{S_{d-1} \bar{\rho}_{\beta}}{2d} \int_0^{\infty} w'(r) p(r) r^{d-1} dr. \quad (\text{F30})$$

For the correction to the pair correlation to be continuous at zero (Eq. (F2)), the solution should satisfy $p(0) = 0$. If the potentials diverge strongly at the origin, this condition can be replaced by $p(\epsilon) = 0$, with small enough $\epsilon > 0$. If the potentials vanish beyond r_c , solving Eq. (F29) for $u = v = 0$ leads to $p(r) \propto r^{1-d}$ for $r > r_c$. This relation can be turned into the relation $p'(r) = \frac{1-d}{r} p(r)$, which may be used as the second boundary condition at $r = r_c$. In the case where the potentials do not vanish beyond a given distance, such as LJ potentials, this boundary condition can still be used with a large enough r_c . These two boundary conditions with the ODE (F29) form a boundary value problem, which may be solved numerically.

[1] Tamás Vicsek and Anna Zafeiris, ‘‘Collective motion,’’ *Physics Reports* **517**, 71–140 (2012).

[2] M. C. Marchetti, J. F. Joanny, S. Ramaswamy, T. B.

- Liverpool, J. Prost, Madan Rao, and R. Aditi Simha, “Hydrodynamics of soft active matter,” *Rev. Mod. Phys.* **85**, 1143 (2013).
- [3] Michael E Cates and Julien Tailleur, “Motility-Induced Phase Separation,” *Ann. Rev. Condens. Matter Phys.* **6**, 219 (2015).
- [4] Clemens Bechinger, Roberto Di Leonardo, Hartmut Löwen, Charles Reichardt, Giorgio Volpe, and Giovanni Volpe, “Active Particles in Complex and Crowded Environments,” *Reviews of Modern Physics* **88**, 045006 (2016).
- [5] Rodrigo Soto and Ramin Golestanian, “Self-Assembly of Catalytically Active Colloidal Molecules: Tailoring Activity Through Surface Chemistry,” *Physical Review Letters* **112**, 068301 (2014).
- [6] Rodrigo Soto and Ramin Golestanian, “Self-assembly of active colloidal molecules with dynamic function,” *Phys. Rev. E* **91**, 052304 (2015).
- [7] Jaime Agudo-Canalejo and Ramin Golestanian, “Active Phase Separation in Mixtures of Chemically Interacting Particles,” *Physical Review Letters* **123**, 18101 (2019).
- [8] Babak Nasouri and Ramin Golestanian, “Exact Phoretic Interaction of Two Chemically Active Particles,” *Physical Review Letters* **124**, 168003 (2020).
- [9] Suropriya Saha, Jaime Agudo-Canalejo, and Ramin Golestanian, “Scalar Active Mixtures: The Nonreciprocal Cahn-Hilliard Model,” *Physical Review X* **10**, 41009 (2020).
- [10] Zhihong You, Aparna Baskaran, and M. Cristina Marchetti, “Nonreciprocity as a generic route to traveling states,” *Proceedings of the National Academy of Sciences of the United States of America* **117**, 19767–19772 (2020).
- [11] Alberto Dinelli, Jérémy O’Byrne, Agnese Curatolo, Yongfeng Zhao, Peter Sollich, and Julien Tailleur, “Non-reciprocity across scales in active mixtures,” , [arXiv:2203.07757v2](https://arxiv.org/abs/2203.07757v2) (2022), [arXiv:2203.07757](https://arxiv.org/abs/2203.07757).
- [12] Federico Ghimenti, Ludovic Berthier, Grzegorz Szamel, and Frédéric van Wijland, “Sampling efficiency of transverse forces in dense liquids,” (2023), [arXiv:2307.02840](https://arxiv.org/abs/2307.02840) [[cond-mat.soft](https://arxiv.org/abs/2307.02840)].
- [13] Tingting Yu, Prabha Chuphal, Snigdha Thakur, Shang Yik Reigh, Dhruv P. Singh, and Peer Fischer, “Chemical micromotors self-assemble and self-propel by spontaneous symmetry breaking,” *Chemical Communications* **54**, 11933–11936 (2018).
- [14] Jens Grauer, Hartmut Löwen, Avraham Be’er, and Benno Liebchen, “Swarm Hunting and Cluster Ejections in Chemically Communicating Active Mixtures,” *Scientific Reports* **10**, 5594 (2020).
- [15] Ran Niu, Andreas Fischer, Thomas Palberg, and Thomas Speck, “Dynamics of Binary Active Clusters Driven by Ion-Exchange Particles,” *ACS Nano* **12**, 10932–10938 (2018).
- [16] Caleb H. Meredith, Pepijn G. Moerman, Jan Groenewold, Yu Jen Chiu, Willem K. Kegel, Alfons van Blaaderen, and Lauren D. Zarzar, “Predator–prey interactions between droplets driven by non-reciprocal oil exchange,” *Nature Chemistry* **12**, 1136–1142 (2020).
- [17] Michel Fruchart, Ryo Hanai, Peter B. Littlewood, and Vincenzo Vitelli, “Non-reciprocal phase transitions,” *Nature* **592**, 363 (2021).
- [18] N Ganai, S Sengupta, and G I Menon, “Chromosome positioning from activity-based segregation,” *Nucleic Acids Research* **42**, 4145 (2014).
- [19] A. Y. Grosberg and J. F. Joanny, “Nonequilibrium statistical mechanics of mixtures of particles in contact with different thermostats,” *Phys. Rev. E* **92**, 032118 (2015).
- [20] Hidenori Tanaka, Alpha A. Lee, and Michael P. Brenner, “Hot Particles Attract in a Cold Bath,” *Phys. Rev. Fluids* **2**, 043103 (2017).
- [21] Jan Smrek and Kurt Kremer, “Small Activity Differences Drive Phase Separation in Active-Passive Polymer Mixtures,” *Physical Review Letters* **118**, 098002 (2017).
- [22] Efe Ilker and Jean-François Joanny, “Phase separation and nucleation in mixtures of particles with different temperatures,” *Phys. Rev. Research* **2**, 23200 (2020).
- [23] Michael Wang and Alexander Y. Grosberg, “Three-body problem for Langevin dynamics with different temperatures,” *Physical Review E* **101**, 032131 (2020).
- [24] A. V. Ivlev, J. Bartnick, M. Heinen, C. R. Du, V. Nosenko, and H. Löwen, “Statistical mechanics where newton’s third law is broken,” *Physical Review X* **5**, 011035 (2015).
- [25] Yu Jen Chiu and Ahmad K. Omar, “Phase coexistence implications of violating Newton’s third law,” *The Journal of chemical physics* **158**, 164903 (2023).
- [26] Rituparno Mandal, Santiago Salazar Jaramillo, and Peter Sollich, “Robustness of travelling states in generic non-reciprocal mixtures,” , [arXiv:2212.05618v1](https://arxiv.org/abs/2212.05618v1) (2022), [arXiv:2212.05618](https://arxiv.org/abs/2212.05618).
- [27] Felix Höfling and Thomas Franosch, “Anomalous transport in the crowded world of biological cells,” *Rep. Prog. Phys.* **76**, 046602 (2013).
- [28] Carlo Manzo and Maria F Garcia-Parajo, “A review of progress in single particle tracking: from methods to biophysical insights,” *Reports on Progress in Physics* **78**, 124601 (2015).
- [29] Note that taking the limit $X_A \rightarrow 0$ or $X_B \rightarrow 0$ corresponds to the situation of a single tracer coupled non-reciprocally to a bath of particles, which is covered by our approach.
- [30] A A Louis, P G Bolhuis, and J P Hansen, “Mean-field fluid behavior of the Gaussian core model,” *Phys. Rev. E* **62**, 7961 (2000).
- [31] C. N. Likos, A. Lang, M. Watzlawek, and H. Löwen, “Criterion for determining clustering versus reentrant melting behavior for bounded interaction potentials,” *Phys. Rev. E* **63**, 031206 (2001).
- [32] A. Lang, C. N. Likos, M. Watzlawek, and H. Löwen, “Fluid and solid phases of the Gaussian core model,” *Journal of Physics Condensed Matter* **12**, 5087–5108 (2000).
- [33] Note that the enhancement due to non-reciprocity can actually compensate the hindering due to crowding, in such a way that D_{eff}^B may exceed its bare value (i.e. its value in the limit of infinite dilution) denoted by D_B .
- [34] Vincent Démery, Olivier Bénichou, and Hugo Jacquin, “Generalized Langevin equations for a driven tracer in dense soft colloids: construction and applications,” *New J. Phys.* **16**, 053032 (2014).
- [35] C W Gardiner, *Handbook of Stochastic Methods* (Springer, 1985).
- [36] D S Dean, “Langevin equation for the density of a system of interacting Langevin processes,” *J. Phys. A: Math. Gen.* **29**, L613 (1996).
- [37] Alexis Poncet, Olivier Bénichou, Vincent Démery, and Gleb Oshanin, “Universal long ranged correlations in

- driven binary mixtures,” *Phys. Rev. Lett.* **118**, 118002 (2017).
- [38] Vincent Démery and David S. Dean, “Perturbative path-integral study of active- and passive-tracer diffusion in fluctuating fields,” *Phys. Rev. E* **84**, 011148 (2011).
- [39] Marie Jardat, Vincent Dahirel, and Pierre Illien, “Diffusion of a tracer in a dense mixture of soft particles connected to different thermostats,” *Phys. Rev. E* **106**, 064608 (2022).
- [40] Vincent Démery and Étienne Fodor, “Driven probe under harmonic confinement in a colloidal bath,” *J. Stat. Mech* **2019**, 033202 (2019).
- [41] H. N. W. Lekkerkerker and J. K. G. Dhont, “On the calculation of the self-diffusion coefficient of interacting Brownian particles,” *J. Chem. Phys.* **80**, 5790–5792 (1984).
- [42] Efe Ilker, Michele Castellana, and Jean-François Joanny, “Long-time diffusion and energy transfer in polydisperse mixtures of particles with different temperatures,” *Phys. Rev. Research* **3**, 023207 (2021).
- [43] Grzegorz Szamel, “Self-propelled particle in an external potential: Existence of an effective temperature,” *Physical Review E* **90**, 012111 (2014).
- [44] P. Romanczuk, M. Bär, W. Ebeling, B. Lindner, and L. Schimansky-Geier, “Active Brownian particles: From individual to collective stochastic dynamics: From individual to collective stochastic dynamics,” *European Physical Journal: Special Topics* **202**, 1–162 (2012).
- [45] Alexandre Solon and Jordan M. Horowitz, “On the Einstein relation between mobility and diffusion coefficient in an active bath,” *J. Phys. A: Math. Theor.* **55**, 184002 (2022).
- [46] Deborah Schwarcz and Stanislav Burov, “Emergence of directed motion in a crowded suspension of overdamped particles,” (2023), [arXiv:2304.12724](https://arxiv.org/abs/2304.12724).
- [47] Bradley R. Parry, Ivan V. Surovtsev, Matthew T. Cabeen, Corey S. O’Hern, Eric R. Dufresne, and Christine Jacobs-Wagner, “The bacterial cytoplasm has glass-like properties and is fluidized by metabolic activity,” *Cell* **156**, 183–194 (2014).
- [48] <https://www.lammps.org>, accessed: Oct 2023.
- [49] Steve Plimpton, “Fast parallel algorithms for short-range molecular dynamics,” *Journal of Computational Physics* **117**, 1–19 (1995).
- [50] A. P. Thompson, H. M. Aktulga, R. Berger, D. S. Bolintineanu, W. M. Brown, P. S. Crozier, P. J. in ’t Veld, A. Kohlmeyer, S. G. Moore, T. D. Nguyen, R. Shan, M. J. Stevens, J. Tranchida, C. Trott, and S. J. Plimpton, “LAMMPS - a flexible simulation tool for particle-based materials modeling at the atomic, meso, and continuum scales,” *Comp. Phys. Comm.* **271**, 108171 (2022).
- [51] P M Chaikin and T C Lubensky, *Principles of condensed matter physics* (Cambridge University Press).
- [52] Urna Basu, Vincent Démery, and Andrea Gambassi, “Dynamics of a colloidal particle coupled to a Gaussian field: from a confinement-dependent to a non-linear memory,” *SciPost Phys.* **13**, 078 (2022).